2011

Calculations of the Temperature and Alloy Composition Effects on the Optical Properties of Alx Ga1-x Asy Sb1-y and Gax In1-x Asy Sb1-y in the Spectral Range 0.5-6 eV

Juan A. Gonzalez-Cuevas
Old Dominion University

Tamer F. Refaat
Old Dominion University

M. Nurul Abedin
Old Dominion University

Hani E. Elsayed-Ali
Old Dominion University, helsayed@odu.edu

Original Publication Citation

Gonzalez-Cuevas, J. A., Refaat, T. F., Abedin, M. N., & Elsayed-Ali, H. E. (2007). Calculations of the temperature and alloy composition effects on the optical properties of Al_x Ga_{1-x} As_y Sb_{1-y} and Ga_x In_{1-x} As_y Sb_{1-y} in the spectral range 0.5-6 eV. *Journal of Applied Physics, 102*(1), 014504. doi:10.1063/1.2751406

Calculations of the temperature and alloy composition effects on the optical properties of $Al_xGa_{1-x}As_ySb_{1-y}$ and $Ga_xIn_{1-x}As_ySb_{1-y}$ in the spectral range 0.5–6 eV

Juan A. Gonzalez-Cuevas
Department of Electrical and Computer Engineering, Old Dominion University, Norfolk, Virginia 23529

Tamer F. Refaat
Applied Research Center, Old Dominion University, Norfolk, Virginia 23529

M. Nurul Abedin
Passive Sensor Systems Branch, NASA Langley Research Center, Hampton, Virginia 23681

Hani E. Elsayed-Ali[a)]
Department of Electrical and Computer Engineering, and the Applied Research Center, Old Dominion University, Norfolk, Virginia 23529

(Received 9 March 2007; accepted 21 May 2007; published online 5 July 2007)

A detailed analysis is presented on the temperature and alloy composition dependence of the optical properties of III-V alloys $Al_xGa_{1-x}As_ySb_{1-y}$ and $Ga_xIn_{1-x}As_ySb_{1-y}$ in the energy range 0.5–6 eV. Expressions for the complex dielectric function are based on a semiempirical phenomenological model, which takes under consideration indirect and direct transitions below and above the fundamental absorption edge. Dielectric function and absorption coefficient calculations are in satisfactory agreement with available experimental data. Other dielectric related optical data, such as the refractive index, extinction, and reflection coefficients, can also be obtained from the model.
 [DOI: 10.1063/1.2751406]

I. INTRODUCTION

AlGaAsSb and InGaAsSb are semiconductor materials of increasing technological importance to optoelectronic devices. A detailed knowledge of their optical properties is essential for the design and fabrication of heterojunction photodetectors, thermophotovoltaic cells, infrared light-emitting diodes, fiber optics, and injection lasers.[1–3]

The optical response of a material in terms of the incident radiation frequency (ν) is fully described by the complex dielectric function $\varepsilon(\nu)=\varepsilon_1(\nu)+i\varepsilon_2(\nu)$, where the real and imaginary parts are related by the Kramers-Kronig transformation.[1] The dielectric function is experimentally determined using various techniques, such as spectroscopic ellipsometry, reflectance measurements, and electron-energy-loss spectroscopy.[1] Unfortunately, experimental measurements are not expressed as continuous analytic functions of the photon energy of the incident radiation. Modeling of the experimental dielectric function in terms of photon energy thus becomes crucial in the quantitative interpretation of the measured optical response, which helps in improving optoelectronic device design.

Several methods have been proposed in the literature for modeling the dielectric function. Depending on the approach taken, the different models can be classified as quantum mechanical or semiempirical in nature. Strict quantum-mechanical models utilize *ab initio* or first-principle calculations to obtain both the real and imaginary parts of the dielectric function, considering the electron-hole pair interactions, i.e., the excitonic effects. Semi-quantum-mechanical models use first-principle calculations for the imaginary part of the dielectric function. Then, the Kramers-Kronig transformation is used to get the real part of the dielectric function from the imaginary part.[1]

Semiempirical approaches for calculating the dielectric function include the damped harmonic oscillator model (DHO),[4] the standard critical points model (SCP),[5] the models by Fourouhi and Bloomer,[6] Adachi,[7–10] Holden *et al.*,[11] and Kim and Sivananthan.[12]

The DHO model describes the dielectric function in a phenomenological manner with the finite sum of Lorentz oscillators,[4]

$$\varepsilon(\nu) = 1 - \sum_{j=1}^{N} A_j \left(\frac{1}{h\nu + h\nu_j + i\Gamma_j} - \frac{1}{h\nu - h\nu_j + i\Gamma_j} \right), \quad (1)$$

where h is Planck's constant, $h\nu$ is the photon energy of the incident radiation, Γ_j is the adjustable damping constant (a phenomenological linewidth), A_j is the fitted strength parameter, and $h\nu_j$ is the oscillator energy. The fitting improves with an increase in the number of oscillators, which in turn increases the number of adjustable parameters needed. The DHO model is not appropriate for describing the derivatives of the dielectric function, which allow a better determination of the critical points (CP) of the energy levels. Moreover, it has low accuracy below the fundamental band gap (E_0).[1] Also, parameters are generally not related to the band structure.

The SCP model takes into account the contributions from each critical point with analytical line shapes,[5]

[a)]Electronic mail: helsayed@odu.edu

$$\varepsilon(\nu) = \sum_{j=1}^{N} [C_j - A_j \exp(i\phi_j)(h\nu - h\nu_j + i\Gamma_j)^n], \quad (2)$$

where the CP is described by an amplitude A_j, nonresonant contribution C_j, lifetime broadening (or damping constant) Γ_j, CP energy threshold $h\nu_j$, and excitonic phase angle ϕ_j. $h\nu$ and Γ_j have similar meanings as in Eq. (1), but in this case correspond to a particular CP instead of an oscillator. The exponent n is equal to $-\frac{1}{2}$ for one-dimensional (1D) CPs, $n=0$ [logarithmic, i.e., $\ln(h\nu - h\nu_j + i\Gamma)$] for two-dimensional (2D) CPs, $n=\frac{1}{2}$ for three-dimensional (3D) CPs, and $n=-1$ for discrete excitons with Lorentzian line shape.[5] The SCP model fits well to the derivatives of the dielectric function, but only moderately to the dielectric function itself.[1]

The model of Forouhi and Bloomer[6] is based on the quantum-mechanical theory of absorption. While the model has simple equations with a low number of parameters, only one parameter from the electronic band gap, E_0, is considered. The model is not appropriate for describing the derivatives of the dielectric function, and has low accuracy below E_0.[1]

The dielectric function model proposed by Adachi[7–10] combines both the SCP model for the lowest energy levels and the DHO model for higher photon energy with undefined CPs [Eqs. (1) and (2)]. Contributions from indirect transitions and discrete and continuum excitons can be considered if needed, depending on the material. Adachi's model is relatively simple, since all expressions are analytical in nature. Unfortunately, it is not very accurate around E_0. It also presents overestimation of the exciton related model parameters because the parameters for bound and unbound states are not independent.

Other models include those by Holden *et al.*,[11] and Kim *et al.*[12] The model of Holden *et al.* considers excitons plus band-to-band Coulomb enhanced line shapes near CPs, i.e., the Coulomb interaction between electron and hole. For higher energies, a DHO approximation is used. It expresses the dielectric function analytically and has a small number of parameters. This model is applicable for determining the Rydberg energies for 2D and 3D excitons, but has a number of intricate equations and leads to singularity when $E=0$.[1] An extended absorption tail is produced in ε_2 due to the purely Lorentzian broadening, which has been artificially avoided (as in Adachi's model) using a linear cutoff. To better fit experimental data, Kim *et al.* have considered Gaussian broadening in their model, approximated with a frequency-dependent analytical expression. This model fits well to the dielectric function and its derivatives, but has many intricate equations that are not analytical and require a large number of parameters. The frequency-dependent expression for Γ used by Kim *et al.* was later introduced into different models.[1,13–15]

Results from the quantum-mechanical approach show several discrepancies between the calculations and experimental data.[1] The magnitude, sharpness, and position of the peaks do not necessarily coincide, and there are typically more structures in the computed curves than measured. We thus utilize a semiempirical phenomenological model akin to Adachi's.[7–10] Since our main goal is to obtain the optical properties of AlGaAsSb and GaInAsSb as a function of both composition and temperature over a wide spectral range, more complicated models that introduce too many phenomenological parameters or are not fully expressed analytically are ill suited from a practical standpoint.

This article is organized as follows: Sec. II provides the theoretical model for calculating the dielectric function (Sec. II A), the temperature effects (Sec. II B), compositional dependencies (Sec. II C), and dielectric related optical constants (Sec. II D). In Sec. III, analysis and discussion of the calculated optical properties for both $Al_xGa_{1-x}As_ySb_{1-y}$ (Sec. III A) and $Ga_xIn_{1-x}As_ySb_{1-y}$ (Sec. III B) are given. Finally, conclusions obtained from this work are summarized in Sec. IV.

II. THEORETICAL MODEL

In order to model the optical properties of the quaternary materials under study, the dielectric function is calculated from semiempirical expressions for lower-lying transitions at major critical points in the joint density of states, and oscillators for higher-lying transitions. The final equation for the dielectric function over the spectral region 0.5–6 eV is expressed in terms of critical point energies and unknown parameters (e.g., strengths and lifetime broadenings) which are, to varying degrees, dependent upon composition and temperature. Thus, by carefully considering the variability of these parameters and the inherent relation of the optical constants to the dielectric function, it is possible to model the thermal and alloy composition effects on the optical properties of GaInAsSb and AlGaAsSb, the details of which are given in the following subsections.

A. Dielectric function calculation

The dielectric function of III-V semiconductors with a zinc-blende-type structure is dependent upon various transitions in energy levels deep in the valence band. In this work, we have considered transitions in the direct gap (E_0), spin-orbit split component ($E_0+\Delta_0$), spin-orbit split doublet (E_1, $E_1+\Delta_1$), higher-lying E_2 peak, and indirect gap E_g^{ID} (E_X or E_L), which were found to offer the most significant contributions. Figure 1 illustrates the various transitions being considered for the case of the energy band structure of the $Al_xGa_{1-x}Sb$ ternary compound in the AlSb-rich composition domain.[16]

We next discuss the various transitions involved. The contribution of the $E_0(\Gamma)$ and $[E_0(\Gamma)+\Delta_0(\Gamma)]$ energy gap involve transitions from 3D M_0-type critical points and take place at the center point Γ of the Brillouin zone. Assuming parabolic bands, their contributions to the dielectric function are given by[4,10]

$$\varepsilon^I(\nu) = AE_0^{-1.5}\left[f\left(\frac{h\nu + i\Gamma}{E_0}\right) + \frac{1}{2}\left(\frac{E_0}{E_0+\Delta_0}\right)^{1.5} f\left(\frac{h\nu + i\Gamma}{E_0+\Delta_0}\right)\right], \quad (3)$$

where

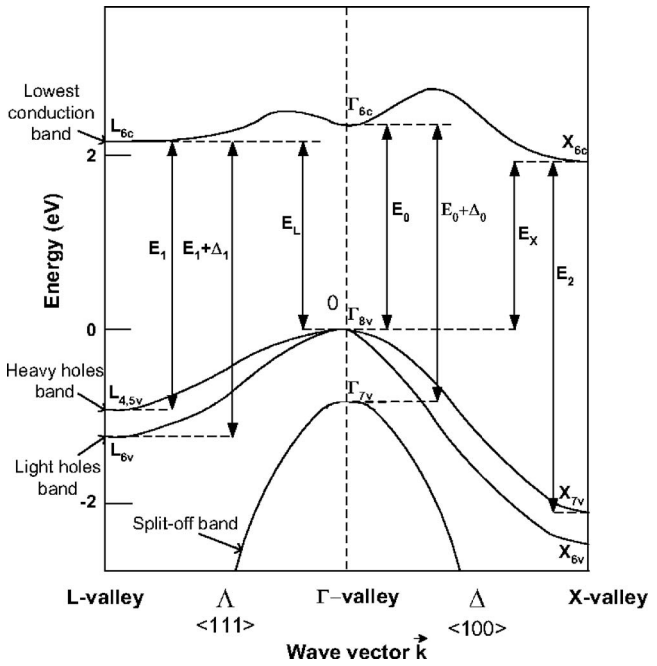

FIG. 1. Electronic energy-band structure of $Al_xGa_{1-x}Sb$ in the AlSb-rich domain along several lines of high-symmetry direction, highlighting the transitions considered in the model (After Ref. 16).

$$f(z) = z^{-2}[2 - (1+z)^{0.5} - (1-z)^{0.5}]. \tag{4}$$

A is a strength parameter dependent on the combined density of states mass m^* and the squared momentum matrix element P^2, i.e, $A = (4/3)(3m^*/2)^{1.5}P^2$. For each transition, the damping constant Γ in the equations accounts for lifetime broadening.

The $E_1(\Lambda)$ and $[E_1(\Lambda)+\Delta_1(\Lambda)]$ transitions are from the 3D M_1 CPs and take place along the $\langle 111\rangle$ directions (Λ) or at L points in the Brillouin zone. Since the longitudinal effective mass is much larger than the transverse counterpart, the contributions of these transitions to the dielectric function can be treated as a 2D minima M_0 as follows:[4,10]

$$\varepsilon^{II}(\nu) = -B_1\left(\frac{h\nu + i\Gamma}{E_1}\right)^{-2}\ln\left[1 - \left(\frac{h\nu + i\Gamma}{E_1}\right)^2\right] - B_2\left(\frac{h\nu + i\Gamma}{E_1 + \Delta_1}\right)^{-2}\ln\left[1 - \left(\frac{h\nu + i\Gamma}{E_1 + \Delta_1}\right)^2\right]. \tag{5}$$

For zinc-blende-type semiconductors, the strength parameters B_1 and B_2 are given by[17]

$$B_1 = 44\frac{E_1 + \frac{\Delta_1}{3}}{a_{lc}E_1^2}, \tag{6}$$

$$B_2 = 44\frac{E_1 + \frac{2\Delta_1}{3}}{a_{lc}(E_1 + \Delta_1)^2}, \tag{7}$$

where a_{lc} is the lattice constant, which expands with temperature. The above equations for B_1 and B_2 allow a better introduction of external perturbations, such as temperature, pressure, or electric field variations.

The transition from the $E_2(X)$ gap corresponds to a well-defined critical point. Thus, it is characterized by a Lorentz-type damped harmonic oscillator,[5,10]

$$\varepsilon^{III}(\nu) = \frac{CE_2^2}{E_2^2 - (h\nu)^2 - ih\nu\Gamma}, \tag{8}$$

where C is a nondimensional (i.e., constant) strength parameter.

The transition from the indirect band gap E_g^{ID} is expressed as a second-order process in the perturbation, giving[10]

$$\varepsilon^{IV}(\nu) = \frac{2D}{\pi}\left\{-\frac{(E_g^{ID})^2}{(h\nu + i\Gamma)^2}\ln\left(\frac{E_c}{E_g^{ID}}\right) + \frac{1}{2}\left(1 + \frac{E_g^{ID}}{h\nu + i\Gamma}\right)^2\ln\left(\frac{h\nu + i\Gamma + E_c}{h\nu + i\Gamma + E_g^{ID}}\right) + \frac{1}{2}\left(1 - \frac{E_g^{ID}}{h\nu + i\Gamma}\right)^2\ln\left(\frac{h\nu + i\Gamma - E_c}{h\nu + i\Gamma - E_g^{ID}}\right)\right\}. \tag{9}$$

Here, D is the indirect gap strength parameter independent of the photon energy, and E_c is a high-energy cutoff, assumed equal to E_1, which prevents nonphysical parabolic bands extending to infinite energies.

Finally, adding all individual contributions, from Eqs. (3), (5), (8), and (9), gives the complex dielectric function,

$$\varepsilon(\nu) = \varepsilon^{I}(\nu) + \varepsilon^{II}(\nu) + \varepsilon^{III}(\nu) + \varepsilon^{IV}(\nu). \tag{10}$$

The Levenberg-Marquardt algorithm[18,19] was used to fit all unknown model parameters through minimization of the cost function χ^2 (least-squares-fitting procedure) over all available experimental data points N at different temperatures and alloy composition,

$$\chi^2 = \frac{1}{2}\sum_{i=1}^{N}\{[\varepsilon_1^{\text{calc}}(\nu_i) - \varepsilon_1^{\text{exp}}(\nu_i)]^2 + [\varepsilon_2(\nu_i)^{\text{calc}} - \varepsilon_2^{\text{exp}}(\nu_i)]^2\}, \tag{11}$$

where the superscripts calc and exp stand for calculated and experimental dielectric function values, both corresponding to a particular ith photon energy.

Experimental dielectric function data at 300 K were obtained from Refs. 20 and 21 for GaAs, GaSb, InAs, and InSb; Ref. 22 for AlAs; Ref. 23 for AlSb, Ref. 24 for $Al_xGa_{1-x}As$, Ref. 25 for $In_xGa_{1-x}As$, and Ref. 26 for $Ga_xIn_{1-x}As_ySb_{1-y}$. Dielectric data for various temperatures were taken from Refs. 27–31 for AlAs, InSb, GaAs, GaSb, and $Al_xGa_{1-x}As$.

Table I provides fitted parameters used in the calculation of the dielectric function for each binary compound. From the simulations conducted, these parameters were found to have a negligible effect on the temperature variation of the dielectric constant, and thus have been assumed to remain constant. Remaining dielectric function parameters with greater temperature dependency, such as critical point energies and lifetime broadenings, are detailed in the following section.

TABLE I. Basic fitted parameters used in the calculation of the dielectric function of each binary compound.

Parameter	AlAs	AlSb	InAs	InSb	GaAs	GaSb
$A[E_0(\Gamma)/E_0(\Gamma)+\Delta_0(\Gamma)]$ ($eV^{1.5}$)	23.740	36.580	19.950	16.830	5.520	1.102
$C[E_2(X)]$	2.240	1.600	1.750	2.640	2.890	3.340
$D[E_g^{ID}]$	0.705	1.190	21.511	38.830	21.320	4.93
$\Gamma[E_0(\Gamma)/E_0(\Gamma)+\Delta_0(\Gamma)]$ (eV)	0.001	0.001	8.660	4.200	0.001	0.001
$\Gamma[E_g^{ID}]$ (eV)	0.490	1.940	0.350	0.560	0.037	0.020

B. Temperature effects

The dielectric function is strongly connected with the electronic energy band structures of the material. The variation of the critical point energy levels due to lattice thermal expansion and cation-phonon interactions (Debye-Waller effect) is described by the semi-empirical Varshni equation:[32]

$$E(T) = E(T=0) - \frac{\delta T^2}{(T+\beta)}, \tag{12}$$

where $E(T=0)$ is the energy value extrapolated to absolute zero temperature; δ and β are fitting constants. Table II shows the parameters used in Varshni's equation.

Critical point peaks in dielectric function versus photon energy curves exhibit both a vertical and sideways shift with temperature variation.[27–31] Substituting Eq. (12) in the dielectric function expressions given above [Eqs. (3) and (10)] mostly accounts for the horizontal displacement of the criti-

TABLE II. Parameters used in Varshni's expression [Eq. (12)] to calculate the temperature dependence of the critical-point energies of each binary.

	AlAs				AlSb			
Critical point energies	$E(0)$ (eV)	α (meV/K)	β (K)	Ref.	$E(0)$ (eV)	α (meV/K)	β (K)	Ref.
$E_0(\Gamma)$	3.09	0.88	530	33	2.39	0.42	140	33
$E_0(\Gamma)+\Delta_0(\Gamma)$	3.37	0.88[a]	530[a]	33	3.06	0.42[a]	140[a]	33
$E_1(\Lambda)$	3.98	0.67	0	27	2.94	0.47	0	34
$E_1(\Lambda)+\Delta_1(\Lambda)$	4.18	0.67	0	27	3.43	0.43	0	34
E_2(X)	4.86	0.32	0	27	4.18	0.47[c]	0[c]	10
E_g^{ID}	2.46[b]	0.61	204	33	1.70[d]	0.39	140	10 and 33

	InAs				InSb			
Critical point energies	$E(0)$ (eV)	α (meV/K)	β (K)	Ref.	$E(0)$ (eV)	α (meV/K)	β (K)	Ref.
$E_0(\Gamma)$	0.42	0.28	93	33	0.24	0.32	170	33
$E_0(\Gamma)+\Delta_0(\Gamma)$	0.79	0.34[a]	248[a]	33	1.20	0.32[a]	170[a]	33
$E_1(\Lambda)$	2.61	0.50	0	35	2.00	0.68	132	28
$E_1(\Lambda)+\Delta_1(\Lambda)$	2.88	0.50[c]	0[c]	35	2.49	0.65	170	28
E_2(X)	4.74	0.56	0	35	4.24	0.54	0	28
E_g^{ID}	1.13[b]	0.28	93	33	0.93[b]	0.32[a]	170[a]	33

	GaAs				GaSb			
Critical point energies	$E(0)$ (eV)	α (meV/K)	β (K)	Ref.	$E(0)$ (eV)	α (meV/K)	β (K)	Ref.
$E_0(\Gamma)$	1.52	0.55	225	29	0.81	0.42	140	30
$E_0(\Gamma)+\Delta_0(\Gamma)$	1.85	0.35	225	29	1.57	0.42[a]	140[a]	30
$E_1(\Lambda)$	3.04	0.72	205	29	2.19	0.68	147	30
$E_1(\Lambda)+\Delta_1(\Lambda)$	3.27	0.72[c]	205[c]	29	2.62	0.67	176	30
E_2(X)	5.13	0.66	43	29	4.32	0.90	376	30
E_g^{ID}	1.82[b]	0.61	204	33	0.88[b]	0.60	140	30

[a]Temperature variance close to lowest direct gap shift, i.e., Δ_0 relatively constant.
[b]Temperature variance assumed equal to E_1 shift.
[c]$E_L(\Gamma_{8V} \rightarrow L_{6C})$.
[d]$E_X(\Gamma_{8V} \rightarrow X_{6C})$.

TABLE III. Fitted parameters for the temperature dependence of the critical point energy lifetime broadenings [Eq. (13)] of binaries.

	AlAs		AlSb[a]		InAs[a]		InSb		GaAs		GaSb	
Critical point energies	Γ_L (meV)	γ (meV/K)	Γ_L (meV)	γ (meV/K)	Γ_L (meV)	γ (meV/K)	Γ_L (meV)	γ (meV/K)	Γ_L (meV)	γ (meV/K)	Γ_L (meV)	γ (meV/K)
$E_1(\Lambda)/E_1(\Lambda)+\Delta_1(\Lambda)$	0.006	0.029	0.001	0.057	0.25	0.3	0.15	0.28	0.001	0.066	0.001	0.124
$E_2(X)$	742.1	0.164	693	0.306	403	0.3	633.9	0.49	663.1	0.41	680.4	0.48

[a]Temperature behavior assumed similar to binaries with close energy bands, i.e., AlAs for AlSb and InSb for InAs.

cal points toward higher energy with decreasing temperature. Sharpening of E_1, $E_1+\Delta_1$, and E_2 peaks at low temperatures is determined by a reduction of lifetime broadening of the hyperbolic excitons associated with Λ and X, which is approximated with the following linear function:[28]

$$\Gamma(T) = \Gamma_L + \gamma T, \tag{13}$$

where both Γ_L and γ are fitted constants. The first term represents the lifetime broadening caused by temperature-independent mechanisms.[31] Fitted values for Γ_L and γ are listed in Table III. Considering dielectric function, data at 300 K $\Gamma_{(E1/E1+\Delta1)}$ and $\Gamma_{(E2)}$ were found to be 0.017 and 0.785 eV for AlSb and 0.0903 and 0.493 eV for InAs, respectively.[21,22,24] Their temperature dependence was assumed to be similar to the other binaries due to a lack of experimental dielectric-temperature data for these two compounds.

The lattice constant [a_{lc} in Eqs. (6) and (7)] expands linearly with increasing temperature, as given by the following expression:[33]

$$a_{lc}(T) = a_{lc}(300) + \kappa(T - 300), \tag{14}$$

where the first term represents the lattice constant at 300 K and κ is a temperature coefficient. Parameter values in Eq. (14) were taken from Ref. 33 and are listed in Table IV.

C. Composition dependence

The quaternary material $A_xB_{1-x}C_yD_{1-y}$ is constructed of four binary compounds: AC, AD, BC, and BD; or else of four ternary compounds: $A_xB_{1-x}C$, $A_xB_{1-x}D$, AC_yD_{1-y}, and BC_yD_{y-1}. In particular, for AlGaAsSb with form $A_xB_{1-x}C_yD_{1-y}$, its binary compounds are AC=AlAs, AD=AlSb, BC=GaAs, and BD=GaSb. Its ternary compounds are ABC=AlGaAs, ABD=AlGaSb, ACD=AlAsSb, and BCD=GaAsSb. Considering GaInAsSb with form $A_xB_{1-x}C_yD_{1-y}$, the binary compounds are AC=GaAs, AD=GaSb and BC=InAs and BD=InSb. The ternary compounds are ABC=GaInAs, ABD=GaInSb, ACD=GaAsSb, and BCD=InAsSb.

TABLE IV. Parameters used in Eq. (14) for the temperature dependence of the lattice constant of binary compounds (Ref. 33).

	AlAs	AlSb	GaAs	GaSb	InAs	InSb
a_{lc}(Å)	5.66	6.13	5.65	6.10	6.06	6.48
$\kappa(10^{-5}$ Å)	2.90	2.60	3.88	4.72	2.74	3.48

The material parameters for ternary semiconductors (T) in the form $A_xB_{1-x}C$ are commonly obtained from the linear interpolation of the transition parameters of the binary materials (B) using Vegard's law,[36,37]

$$T_{ABC}(x) = xB_{AC} + (1-x)B_{BC} - x(1-x)C, \tag{15}$$

where C is a bowing constant that accounts for deviations from the linear interpolation due to lattice disorders arising from the presence of different cations.

Once the ternary parameters are known via interpolation, the quaternary parameters (Q) for the lower energy levels (alloy in the form $A_xB_{1-x}C_yD_{1-y}$) are obtained using the method of Glisson *et al.*,[38,39]

$$\begin{aligned} Q_{ABCD}(x,y) = \frac{1}{x(1-x)+y(1-y)}\{&x(1-x)[yT_{ABC}(x) \\ &+ (1-y)T_{ABD}(x)] + y(1-y)[xT_{ACD}(y) \\ &+ (1-x)T_{BCD}(y)]\} \end{aligned} \tag{16}$$

The quaternary material parameters (form $A_xB_{1-x}C_yD_{1-y}$) may also be obtained from the binary parameters using Vegard's rule,[36,39]

$$\begin{aligned} Q_{ABCD}(x,y) = &xyB_{AC} + x(1-y)B_{AD} + (1-x)yB_{BC} \\ &+ (1-x)(1-y)B_{BD} + C_{A-B}x(1-x) \\ &+ C_{C-D}y(1-y). \end{aligned} \tag{17}$$

In the above expression, bowing parameters C_{A-B} and C_{C-D} are assumed to arise from independent anion-cation sublattice disorders. Since bowing constants for critical point energies of several ternary III-V semiconductors are available in the literature, we shall then calculate the quaternary energy transitions by making use of Eqs. (15) and (16). For all other model parameters, Eq. (17) is used, with both C_{A-B} and C_{C-D} fitted to experimental data.[20–26] Temperature is assumed to have a negligible effect on bowing parameters, since, as of yet, there is no significant data analysis or analytic interpretation in this regard for several materials.[33]

Table V gives the bowing constants used in the calculation of the various critical point energy transitions for each ternary. Unknown bowing parameters for the indirect band gap are estimated as follows:[39]

$$C(E_g^{ID}) \approx 1/2[C(E_0) + C(E_1)], \tag{18}$$

where $C(E_0)$ and $C(E_1)$ are the bowing parameters for the E_0 and E_1 gaps.

For the spin split-off band, the following approximation is used:[39]

TABLE V. Bowing parameters (in eV) used in the linear interpolation of the critical-point energies for each ternary compound [Eq. (15)] of AlGaAsSb and InGaAsSb at 300 K.

	Bowing parameter (eV)					
Ternary	$C(E_0)$	$C(E_0+\Delta_0)$	$C(E_1)$	$C(E_1+\Delta_1)$	$C(E_2)$	$C(E_g^{ID})$
$Al_xAs_{1-x}Sb$	0.72[a]	0.15[a]	⋯	⋯	⋯	0.28[b]
$GaAs_xSb_{1-x}$	1.20[c]	0.61[a]	⋯	⋯	⋯	1.09[d]
$InAs_xSb_{1-x}$	0.58[e]	1.20[f]	0.55[e]	0.40[e]	0.60[e]	0.57[d]
$Al_xGa_{1-x}As$	0.37[g]	0.07[f]	0.45[f]	⋯	0.02[f]	0.06[g]
$Ga_xIn_{1-x}As$	0.61[h]	0.20[f]	0.50[e]	0.49[e]	0.27[e]	0.72[i]
$Al_xGa_{1-x}Sb$	0.69[j]	0.30[j]	0.28[j]	0.32[k]	⋯	0.55[j]
$Ga_xIn_{1-x}Sb$	0.42[l]	0.10[l]	0.38[e]	0.28[e]	0.24[e]	0.38[d]

[a]Reference 43.
[b]Reference 44.
[c]Reference 45.
[d]Estimated in this study. See the text.
[e]Reference 46.
[f]Reference 47.
[g]Reference 48.
[h]Reference 49.
[i]Reference 50.
[j]Reference 14.
[k]Reference 51.
[l]Reference 52.

$$C(\Delta_0) \approx (\Delta_{01}/E_1)C(E_0), \tag{19}$$

where Δ_{01} and E_1 are the linearly interpolated values at $x=0.5$ of Δ_0 and E_0 from the limiting compounds. Table VI lists the bowing parameters fitted to Eq. (17) for both quaternaries.

D. Optical coefficients

Once the dielectric function for a certain alloy composition and temperature is determined, the real part of the complex refractive index n and its imaginary part k (the extinction coefficient or attenuation index), can be calculated using the following expressions:[21]

$$n = \left(\frac{(\varepsilon_1^2 + \varepsilon_2^2)^{1/2} + \varepsilon_1}{2} \right)^{1/2}, \tag{20}$$

$$k = \left(\frac{(\varepsilon_1^2 + \varepsilon_2^2)^{1/2} - \varepsilon_1}{2} \right)^{1/2}. \tag{21}$$

The normal incidence reflectivity R and the absorption coefficient α are then expressed in terms of n and k as follows:[21]

TABLE VI. Fitted bowing compositional constants used in the linear interpolation of model parameters [Eq. (17) of the binary compounds of AlGaAsSb and InGaAsSb.

	GaInAsSb		AlGaAsSb	
	C_{A-B}	C_{C-D}	C_{A-B}	C_{C-D}
$A[E_0(\Gamma)/E_0(\Gamma)+\Delta_0(\Gamma)]$ ($eV^{1.5}$)	12.389	0.001	0.012	0.010
$C[E_2(X)]$	−1.648	0.002	0.019	0.010
$D[E_g^{ID}]$	17.938	0.001	0.010	0.010
$\Gamma[E_0(\Gamma)/E_0(\Gamma)+\Delta_0(\Gamma)]$ (eV)	−5.017	−0.002	−0.004	0.010
$\Gamma[E_1(\Lambda)/E_1(\Lambda)+\Delta_1(\Lambda)]$ (eV)	0.231	−0.046	0.033	0.009
$\Gamma[E_2(X)]$ (eV)	0.103	0.058	−0.031	0.009
$\Gamma[E_g^{ID}]$ (eV)	−0.079	−0.014	0.008	0.010
a_0(Å)	−2.813	−0.016	0.002	0.010

$$R = \left| \frac{n - ik - 1}{n - ik + 1} \right|^2 = \frac{(n-1)^2 + k^2}{(n+1)^2 + k^2}, \tag{22}$$

$$\alpha = \frac{4\pi k}{\lambda}, \tag{23}$$

where λ is the wavelength of the incident radiation in vacuum.

III. ANALYSIS AND DISCUSSION

Contributions to the dielectric constant arise from several partitions of the Brillouin zone. The percentiles of each contribution were estimated to be in accordance with those reported in Ref. 40. The L region with corresponding E_1 and E_g^{ID} transition energies contributes approximately 65–70% to the total value of the dielectric constant. The Γ region corresponding to the E_0 transition accounts for 5–10% of the total. The E_2 and E_g^{ID} transitions in the X region account for 15–30% of the total.

We have considered only the dominant indirect transitions, i.e., $E_X(\Gamma_{8V} \rightarrow X_{6C})$ for AlSb and $E_L(\Gamma_{8V} \rightarrow L_{6C})$ for all other binaries. Excitonic states in principle exist at each type of critical point, since Coulomb-type interactions are always present between electrons and holes.[10] In fact, at very low temperatures, the excitonic effects profoundly modify the critical points singularity structure, making the one-electron approximation unsuitable. However, excitonic effects are not observed if the thermal energy exceeds the exciton binding energy or the screening effects push the exciton levels into the continuum of the conduction band. In particular, contributions to the dielectric function from 3D discrete excitonic effects near the E_0 critical point can be neglected because of the narrow spectral range of these transitions.[10,40] Contributions from continuous excitons at the E_0 and higher transitions are very similar to noninteracting electron-hole pair characteristics.[10] Thus, for temperatures of 150 K and above, excitonic effects are not as important and the one-electron approximation becomes suitable for most practical applications.

A. $Al_xGa_{1-x}As_ySb_{1-y}$

The $Al_xGa_{1-x}As_ySb_{1-y}$ quaternary alloy is characterized by a relatively large band gap that covers the wavelength range between the visible and infrared regions (0.57–1.72 μm).[39] The alloys can be grown lattice matched to commercially available binary substrates, such as GaSb, InP, and InAs. However, miscibility gaps may limit the range of homogenous solid-phase alloy compositions.[39] AlGaAsSb lattice matched to GaSb is a natural energy barrier to majority carrier transport and is typically used as a cladding layer of fluoride glass fibers and emitters of heterojunction phototransistors due to its lower refractive index.[33,39]

The alloy systems $Al_xGa_{1-x}As_ySb_{1-y}$/GaSb and $Al_xGa_{1-x}As_ySb_{1-y}$/InAs present a transition between direct and indirect structures at approximately $x \approx 0.45$.[39] The E_0 gap at the Γ point is very close to the E_g^{ID} gap at the L point, causing an injected-electron loss and consequently a large threshold current.[39] Sb-based systems have a relatively high

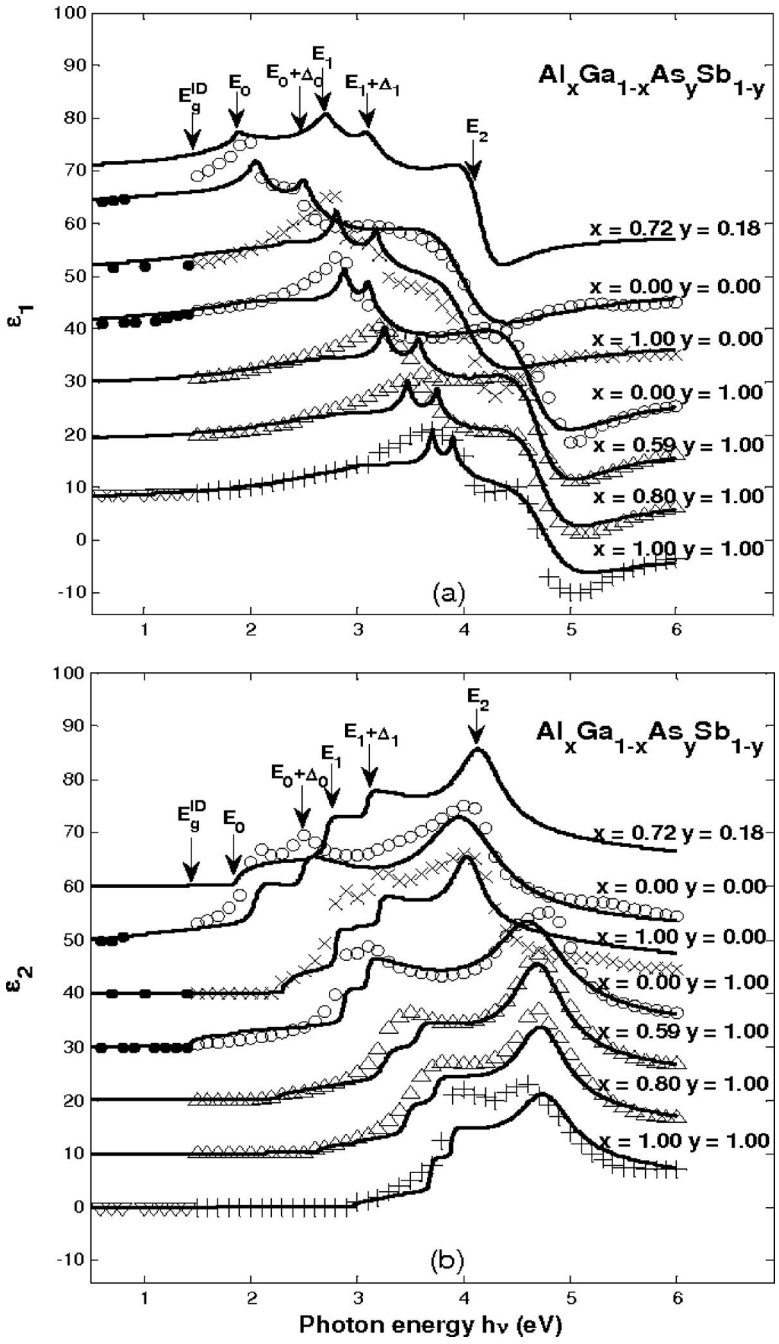

FIG. 2. Real (ε_1) (a) and imaginary (ε_2) (b) components of the dielectric function (ε) of $Al_xGa_{1-x}As_ySb_{1-y}$ at 300 K for various compositions. The solid lines are calculated from the model. Also shown are experimental data points from Ref. 13 (∇), Ref. 20 (○), Ref. 21 (•), Ref. 22 (+), Ref. 23 (×), Ref. 24 (Δ). For clarity, curves are offset by increments of 10 after $x=1$ and $y=1$ composition.

spin split-off gap Δ_0 Auger recombination and intervalence-band optical transitions related to the Δ_0 gap that play an important role in the device operation characteristics, i.e., threshold current and its temperature dependence.[39] AlGaAsSb systems have a large refractive index step within the whole range of alloy composition.

The room-temperature complex dielectric function of the $Al_xGa_{1-x}As_ySb_{1-y}$ alloy is shown in Fig. 2 for six different compositions [real part ε_1, shown in Fig. 2(a) and imaginary part ε_2, shown in Fig. 2(b)]. The solid lines are numerically obtained from the model using Eqs. (3) and (10) to account for the various energy levels contribution, and Eqs. (15) and (17) to calculate the composition dependence of all parameters. Critical point energies are pointed out for the uppermost dielectric curve for $Al_{0.72}Ga_{0.28}As_{0.18}Sb_{0.82}$. The shift of the three dominant structures E_1, $E_1+\Delta_1$, and E_2 to higher energy with increasing Al composition x is evident from looking at the figure. The E_1 and $E_1+\Delta_1$ peaks in the ε_2 spectrum are more resolved at the end points $x=0.00$ and $x=1.00$, while they lose their strengths at intermediate compositions approaching $x\sim0.5$. These broadening dependences are related to statistical fluctuations of the crystal potential in the alloy, which tend to dominate over potential contributions arising from bulk dislocations.[25,37] Reasonable agreement between the modeled dielectric function curves and experimental data is obtained around the lower direct energy gaps E_0 and $E_0+\Delta_0$, indirect band E_g^{ID}, and the higher-lying E_2 CP. In the vicinity of the E_1 and $E_1+\Delta_1$ CPs, calculated curves present somewhat lower and more pronounced peaks than experimental data for both ε_1 and ε_2. Better agreement is obtained if fitted values are used for the strength parameters B_1 and B_2 in Eq. (5) instead of calculat-

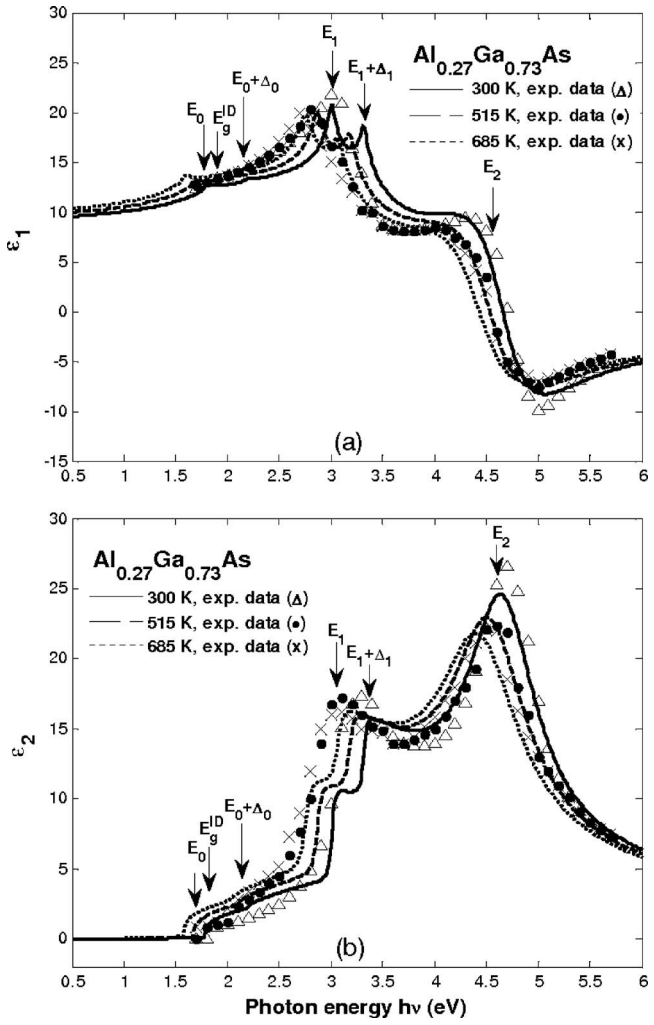

FIG. 3. Real (ε_1) and imaginary (ε_2) components of the dielectric function (ε) of $Al_{0.27}Ga_{0.73}As$ at 300, 515, and 685 K. Calculated values (lines) correspond to experimental data in Ref. 31 (symbols). The arrows highlight the critical point energies at 300 K.

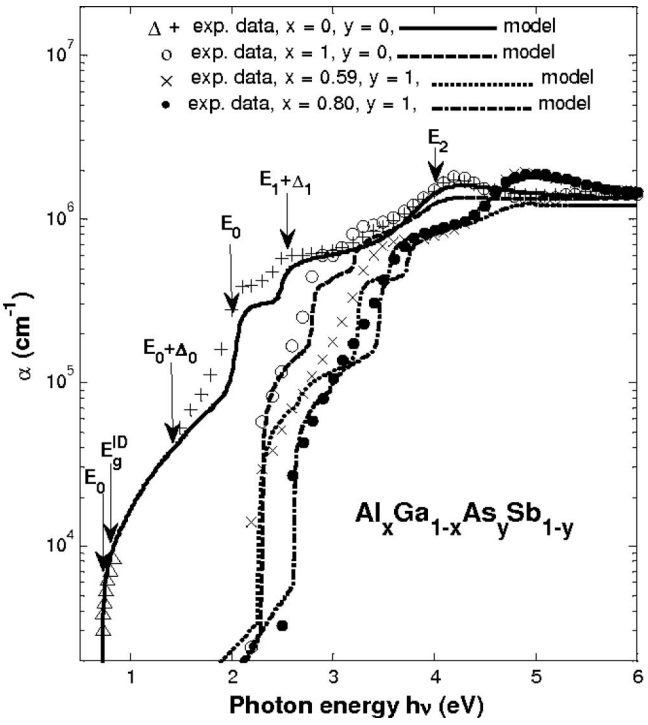

FIG. 4. Absorption coefficient α (of $Al_xGa_{1-x}As_ySb_{1-y}$ at 300 K for various compositions. Experimental data are taken from Ref. 20 (+), Ref. 23 (○), Ref. 24 (×) (•), and Ref. 42 (Δ).

ing them with Eqs. (6) and (7). However, since these expressions for B_1 and B_2 are functions of energy and lattice constant, they allow for a better consideration of temperature effects in a more physical manner while still offering a reasonably good agreement with experiments in light of the crudeness of the theory employed.[17] Moreover, discrepancies exist in the experimental conditions under which the various data considered were obtained. For example, Refs. 20 and 24 present "pseudodielectric: function" data, as they were deduced from reflectance of samples with surface contaminants such as oxides or air pollutants. Taking all these facts and tradeoffs under consideration, the model offers a fairly accurate representation of the dielectric function for various compositions including the temperature effects, and enables the calculation of the optical properties of quaternaries that have not been studied previously. A prediction of the dielectric function for one such quaternary, $Al_{0.72}Ga_{0.28}As_{0.18}Sb_{0.82}$, for which experimental data are not presently available, is also shown in Fig. 2 to demonstrate the capabilities of the model.

Figure 3 depicts the real part ε_1 and imaginary ε_2 components of the dielectric function of $Al_{0.27}Ga_{0.73}As$ at temperatures of 300, 515, and 685 K. Numerical data (lines) are computed using Eqs. (12) and (14) to calculate the temperature dependence of CP energy levels, lifetime broadenings, and lattice expansion, substituted into the dielectric function Eqs. (3) and (10) for every energy level contributions, Composition values are fixed at $x=0.27$ and $y=1$ in Eqs. (15) and (17). Both vertical and horizontal temperature shifts in the CP peaks are clearly visible in Fig. 3. The change in the CP energy levels with temperature, as described by Eq. (12), causes the dielectric function to move sideways. The horizontal shifts in the peaks are more pronounced around the E_1, $E_1+\Delta_1$, and E_2 peaks, corresponding to significant temperature variation in the CP lifetime broadenings around Λ and X, approximated with Eq. (13). In the model, the E_1 and $E_1+\Delta_1$ peaks are also affected by the lattice constant, which expands with increasing temperature. The model is not applicable below 150 K, since the CP energies at very low temperatures are not well known for some of the binary constituents. The energy temperature dependence of these materials was thus assumed linear, which is the case above 150 K.[17,30–32] Moreover, the exact behavior of the energy bands near 0 K, as approximated by Varshni based on earlier estimations, has recently come into question (See, for example, Ref. 41).

Figure 4 shows the room temperature absorption coefficient of $Al_xGa_{1-x}As_ySb_{1-y}$ as a function of photon energy for different compositions. Lines represent the absorption coefficient numerically calculated using Eq. (23). Of great importance is the shift in the cutoff wavelength corresponding to E_0, with lowest and highest values for the binary end points GaSb ($x=0$, $y=0$) and AlAs ($x=1$, $y=1$). Selected absorption experimental data, represented in Fig. 4 by symbols, are

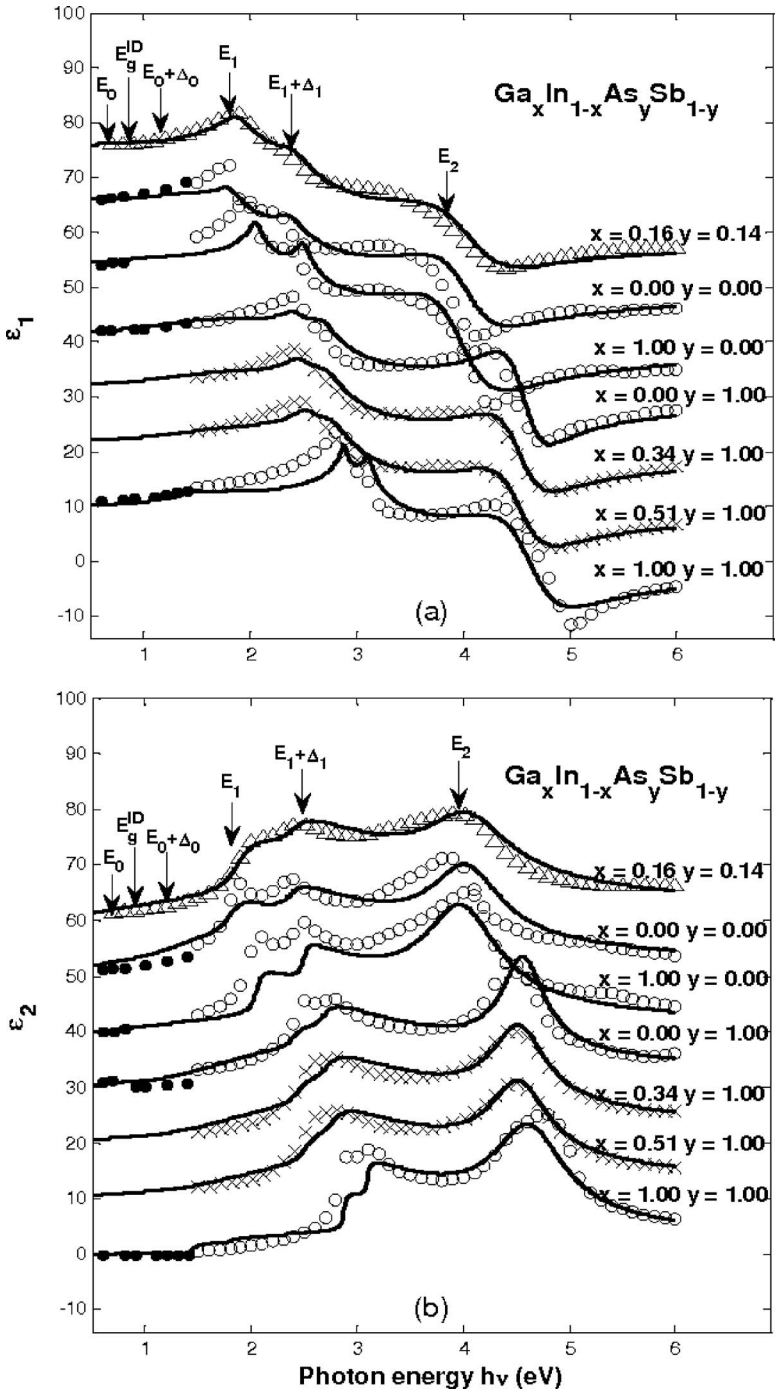

FIG. 5. Real (ε_1) (a) and imaginary (ε_2) (b) components of the dielectric function (ε) of $Ga_xIn_{1-x}As_ySb_{1-y}$ at 300 K for various compositions. The solid lines are calculated from the model. Also shown are selected experimental data points from Ref. 20 (○), Ref. 21 (•), Ref. 25 (×), and Ref. 26 (Δ). For clarity, curves are offset by increments of 10 starting from GaAs.

taken from Refs. 20, 23, 24, and 42. Energy peaks are highlighted in the figure for the uppermost absorption data, corresponding to the GaSb binary.

B. $Ga_xIn_{1-x}As_ySb_{1-y}$

The $Ga_xIn_{1-x}As_ySb_{1-y}$ alloys are suitable for devices operating in the 24 μm spectral region needed for low-loss fluoride glass fibers cores and phototransistor collectors. Like $Al_xGa_{1-x}As_ySb_{1-y}$, $Ga_xIn_{1-x}As_ySb_{1-y}$ may be grown lattice matched on GaSb, InP, and InAs. GaInAsSb lattice matched to GaSb is an important active-region constituent of diode lasers emitting at $\lambda=2$ μm.[33] The cutoff wavelengths of GaInAsSb lattice matched to InP are close to the 1.55 μm low-loss window for optical fiber communications. GaInAsSb/InP usefulness is limited, however, because both end points have nearly the same energy gap (0.71–0.86 eV).[33,39] The band-gap energy varies in the range 0.3–0.71 and 0.36–0.69 eV when lattice matched to GaSb and InAs, respectively. Unlike $Al_xGa_{1-x}As_ySb_{1-y}$, the absorption at the fundamental optical gaps in $Ga_xIn_{1-x}As_ySb_{1-y}$/GaSb and $Ga_xIn_{1-x}As_ySb_{1-y}$/InAs is direct within the whole range of alloy composition.

The quaternary $Ga_xIn_{1-x}As_ySb_{1-y}$ lattice matched to InAs and GaSb presents a refractive index anomaly in the sense that the material with smaller E_0 gap has a lower refractive index, while the opposite behavior is common to most III-V alloys.[39] This is mainly due to alloy disorder effects, i.e., intraband and interband interactions, which break

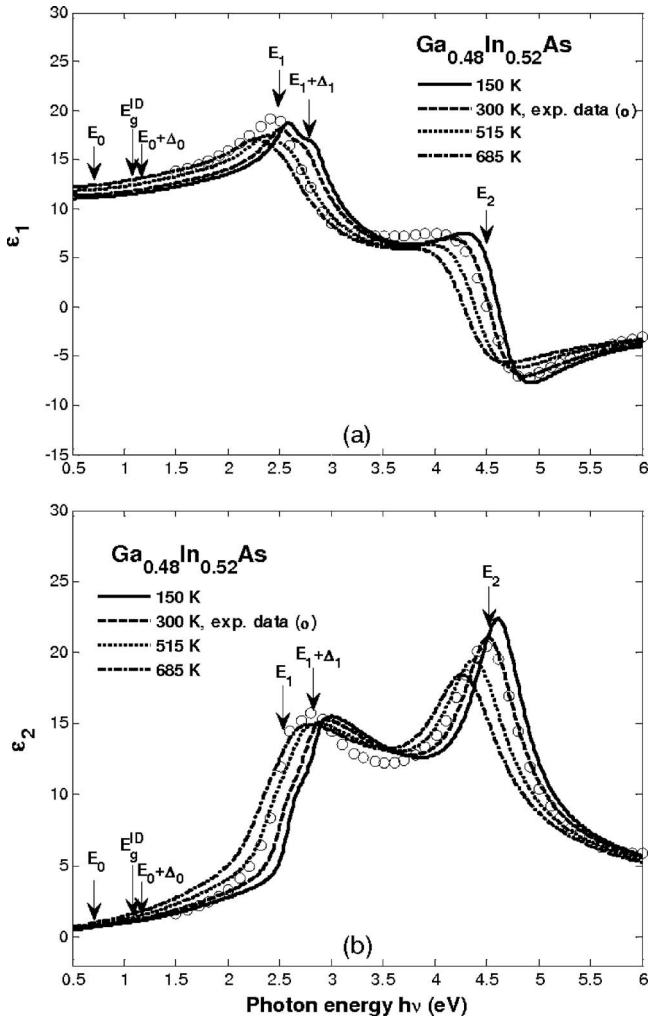

FIG. 6. Real (ε_1) and imaginary (ε_2) components of the dielectric function (ε) of $Ga_{0.48}In_{0.52}As$ at 150, 300, 515, and 685 K. Lines correspond to the fit values obtained from the model. Arrows point toward the critical point energies of dielectric function data at 300 K (from Ref. 23).

the symmetry of the crystal lattice in Sb-based compounds and cause the band structure constants related to the refractive index to present nonlinearity with alloy composition.[39]

The real part ε_1, shown in Fig. 5(a), and imaginary part ε_2, shown in Fig. 5(b), of the complex dielectric function of $Ga_xIn_{1-x}As_ySb_{1-y}$ are calculated for six different compositions at room temperature. The solid lines represent dielectric function calculations using Eqs. (3) and (10) to account for energy gap transitions and Eqs. (15) and (17) to account for the composition dependence, as with $Al_xGa_{1-x}As_ySb_{1-y}$. Curves for each composition are offset by increments of 10 starting from GaAs. Critical point energies are indicated for the uppermost curves. For either GaInAs or GaInSb, CPs E_1, $E_1+\Delta_1$, and E_2 shift to higher energy with increasing x. As is the case for $Al_xGa_{1-x}As_ySb_{1-y}$, the E_1 and $E_1+\Delta_1$ peaks are sharper for $x=0.00$ and $x=1.00$ and weaker at intermediate compositions due to statistical fluctuations of the crystal potential.[25,37] Better agreement with experiments is obtained around E_0, $E_0+\Delta_0$, E_g^{ID}, and E_2, while the E_1 and $E_1+\Delta_1$ CPs have weaker but more pronounced peaks than experiments due to the inclusion of Eqs. (6) and (7) to calculate the B_1 and B_2 strength parameters, the justification of which has been given previously. The accuracy of the calculated results is expected to be similar to the $Al_xGa_{1-x}As_ySb_{1-y}$ case.

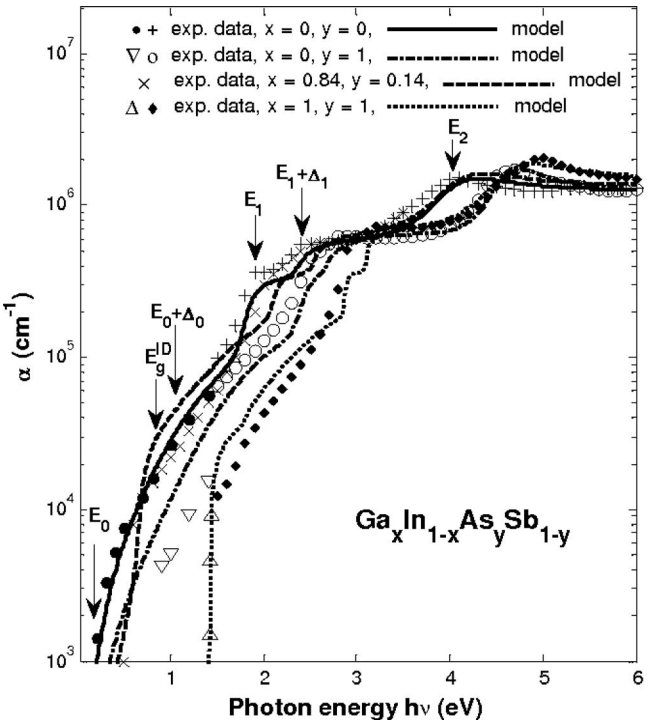

FIG. 7. Absorption coefficient (α) of $Ga_xIn_{1-x}As_ySb_{1-y}$ at 300 K for various compositions. Experimental data are taken from Ref. 20 (+)(○)(♦), Ref. 21 (•)(∇)(Δ), and Ref. 26 (×).

Experimental dielectric function data for the ternaries and quaternaries of $Ga_xIn_{1-x}As_ySb_{1-y}$ at temperatures other than 300 K are not readily available. We thus make a prediction based on the temperature behavior of the binaries and their interpolation. Figure 6 shows the real (ε_1) and imaginary (ε_2) components of the dielectric function of the widely studied ternary $Ga_{0.48}In_{0.52}As$ at 150, 300, 515, and 685 K. Lines correspond to the values obtained from the model, while circles represent room-temperature experimental data taken from Ref. 25. The vertical shift in the peaks of the dielectric function to higher energy with decreasing temperature corresponds to the CP energies increase due to lattice thermal contraction with cooling and cation-phonon interactions, considered in Eq. (12). The horizontal increase in the E_1, $E_1+\Delta_1$, and E_2 peaks with lower temperature is caused by the temperature shift in the CP lifetime broadening parameters with Λ and X [Eq. (13)].

Figure 7 shows the absorption coefficient of $Ga_xIn_{1-x}As_ySb_{1-y}$ at room temperature for several compositions. Lines correspond to values obtained from the model [Eq. (23)]. Selected absorption experimental data, represented in Fig. 7 by symbols, are taken from Refs. 20, 21, and 26. Critical point energies are marked for InSb. The shift in the cutoff photon energy E_0 is lowest for InSb ($x=0$, $y=0$) and highest for GaAs ($x=1$, $y=1$), both binary end points.

IV. CONCLUSIONS

The complex dielectric function and related optical properties of AlGaAsSb and GaInAsSb are analyzed in the

photon-energy range 0.5–6 eV using a semiempirical phenomenological model. The effects of both alloy composition and temperature on the dielectric function are incorporated into the model considering a linear interpolation scheme as well as band gap, broadening, and lattice constant distortions. The methodology for calculation of various device parameters in the AlGaAsSb and GaInAsSb alloy systems is analyzed, and results are presented which could aid in the design of optoelectronic devices.

ACKNOWLEDGMENTS

We would like to thank M. Muñoz and Y.D. Kim for kindly providing us with their experimental data in original digital format.

[1]A. B. Djurisic and E. H. Li, J. Appl. Phys. **89**, 273 (2001).
[2]M. N. Abedin, T. F. Refaat, O. V. Sulima, and U. N. Singh, IEEE Trans. Electron Devices **51**, 2013 (2004).
[3]T. F. Refaat, M. N. Abedin, O. V. Sulima, S. Ismail, and U. N. Singh, Opt. Eng. **43**, 1647 (2004).
[4]M. Erman, J. B. Theeten, P. Chambon, S. M. Kelso, and D. E. Aspnes, J. Appl. Phys. **56**, 2664 (1984).
[5]M. Cardona, *Modulation Spectroscopy* (Academic, New York, 1969), Suppl. 11.
[6]A. R. Forouhi and I. Bloomer, Phys. Rev. B **38**, 1865 (1988).
[7]S. Adachi, Phys. Rev. B **35**, 7454 (1987).
[8]S. Adachi, Phys. Rev. B **38**, 12345 (1988).
[9]S. Adachi, J. Appl. Phys. **66**, 6030 (1989).
[10]S. Adachi, J. Appl. Phys. **67**, 6427 (1990).
[11]T. Holden, P. Ram, and F. H. Pollak, Phys. Rev. B **56**, 4037 (1997).
[12]C. C. Kim and S. Sivananthan, J. Appl. Phys. **78**, 4003 (1995).
[13]A. D. Rakic and M. L. Majewski, J. Appl. Phys. **80**, 5909 (1996).
[14]A. B. Djurišić, E. H. Li, D. Rakic, and M. L. Majewski, Appl. Phys. A: Mater. Sci. Process. **70**, 29 (2000).
[15]A. B. Djurišić, A. D. Rakic, P. C. K. Kwock, E. H. Li, M. L. Majewski, and J. M. Elazar, J. Appl. Phys. **86**, 445 (1999).
[16]C. Alibert, A. Joullie, A. M. Joullie, and C. Ance, Phys. Rev. B **27**, 4946 (1983).
[17]S. Logothetidis, L. Viña, and M. Cardona, Phys. Rev. B **31**, 947 (1985).
[18]K. Levenberg, Q. Appl. Math. **2**, 164 (1944).
[19]D. Marquardt, SIAM J. Appl. Math. **11**, 431 (1963).
[20]D. E. Aspnes and A. A. Studna, Phys. Rev. B **27**, 985 (1983).
[21]B. O. Seraphin and H. E. Bennett, in *Semiconductors and Semimetals*, edited by R. K. Willardson and A. D. Beer (Academic, New York, 1967), Vol. 3, p. 499.
[22]M. Garriga, P. Lautenschlager, M. Cardona, and K. Ploog, Solid State Commun. **61**, 157 (1987).
[23]S. Zollner, C. Lin, E. Schönherr, A. Böhringer, and M. Cardona, J. Appl. Phys. **66**, 383 (1989).
[24]D. E. Aspnes, S. M. Kelso, R. A. Logan, and R. Bhat, J. Appl. Phys. **60**, 754 (1986).
[25]T. J. Kim, T. H. Ghong, Y. D. Kim, S. J. Kim, D. E. Aspnes, T. Mori, T. Yao, and B. H. Koo, Phys. Rev. B **68**, 115323 (2003).
[26]M. Muñoz, K. Wei, F. H. Pollak, J. L. Freeouf, C. A. Wang, and G. W. Charache, J. Appl. Phys. **87**, 1780 (2000).
[27]H. Yao, P. Snyder, K. Stair, and T. Bird, Mater. Res. Soc. Symp. Proc. **242**, 481 (1992).
[28]S. Logothetidis, L. Viña, and M. Cardona, Phys. Rev. B **31**, 947 (1985).
[29]P. Lautenschlager, M. Garriga, S. Logothetidis, and M. Cardona, Phys. Rev. B **35**, 9174 (1987).
[30]S. Zollner, M. Garriga, J. Humlicek, S. Gopalan, and M. Cardona, Phys. Rev. B **43**, 4349 (1991).
[31]S. Logothetidis, M. Cardona, and M. Garriga, Phys. Rev. B **43**, 11950 (1991).
[32]Y. P. Varshni, Physica (Amsterdam) **34**, 149 (1967).
[33]I. Vurgaftman, J. R. Meyer, and L. R. Ram-Mohan, J. Appl. Phys. **89**, 5815 (2001).
[34]A. Joullie, B. Girault, A. M. Joullie, and A. Zien-Eddine, Phys. Rev. B **25**, 7830 (1982).
[35]R. R. L. Zucca and Y. R. Shen, Phys. Rev. B **1**, 2668 (1970).
[36]L. Vegard, Z. Phys. **5**, 17 (1921).
[37]J. A. Van Vechten and T. K. Bergstresser, Phys. Rev. B **1**, 3351 (1970).
[38]C. K. Williams, T. H. Glisson, J. R. Hausser, and M. A. Littlejohn, J. Electron. Mater. **7**, 639 (1978).
[39]S. Adachi, J. Appl. Phys. **61**, 4869 (1987).
[40]M. Linnik and A. Christou, Physica B (Amsterdam) **318**, 140 (2002).
[41]M. Cardona, T. A. Meyer, and M. L. W. Thewalt, Phys. Rev. Lett. **92**, 196403 (2004).
[42]G. Stollwerck, O. V. Sulima, and A. W. Bett, IEEE Trans. Electron Devices **47**, 448 (2000).
[43]M. P. C. M. Krijn, Semicond. Sci. Technol. **6**, 27 (1991), and references therein.
[44]H. Ait Kaci, D. Boukredimi, and M. Mebarki, Phys. Status Solidi A **163**, 101 (1997).
[45]M. B. Thomas, W. M. Coderre, and J. C. Woolley, Phys. Status Solidi A **2**, K141 (1970).
[46]S. S. Vishnubhatla, B. Eyglunent, and J. C. Woolley, Can. J. Phys. **47**, 1661 (1969).
[47]O. Berolo, J. C. Woolley, and J. A. van Vechten, Phys. Rev. B **8**, 3794 (1973).
[48]H. J. Lee, L. Y. Juravel, J. C. Woolley, and A. J. String-Thorpe, Phys. Rev. B **21**, 659 (1980).
[49]K. R. Schulze, H. Neumann, and K. Unger, Phys. Status Solidi B **75**, 493 (1976).
[50]W. Porod and D. K. Ferry, Phys. Rev. B **27**, 2587 (1983).
[51]C. Ance, J. Robin, A. Nguyen Van Mau, and G. Bougnot, J. Phys. C **8**, 1979 (1975).
[52]D. Auvergne, J. Camassel, H. Mathieu, and A. Joullie, J. Phys. Chem. Solids **35**, 133 (1974).